CrossMark

Peer Reviewed

Microstructure and Wear Resistance of Plasma-Sprayed Molybdenum Coating Reinforced by MoSi$_2$ Particles

Jianhui Yan, Zheyu He, Yi Wang, Jingwen Qiu, and Yueming Wang

Mo coatings with or without incorporated MoSi$_2$ were fabricated by atmospheric plasma spraying, and their microstructure, microhardness, bond strength, and wear resistance were compared. Two kinds of spray powder, i.e., pure Mo and a blend of Mo and MoSi$_2$, were sprayed onto low-carbon steel. Microstructural analysis of the MoSi$_2$-Mo coating showed MoSi$_2$ homogeneously distributed in a Mo matrix. Addition of MoSi$_2$ particles increased the microhardness of the as-sprayed Mo coating. The adhesion strength of the Mo coating was better than that of the MoSi$_2$-Mo coating. Wear test results showed that the wear rate and friction coefficient of the two coatings increased with increasing load, and the friction coefficient of the MoSi$_2$-Mo coating was lower than that of the Mo coating. The MoSi$_2$-Mo composite coating exhibited better wear resistance than the Mo coating. The wear failure mechanisms of the two coatings were local plastic deformation, delamination, oxidation, and adhesion wear.

1. Introduction

Molybdenum has characteristics of high thermal conductivity, low thermal expansion coefficient, and very good creep properties at high temperature. It is well known that the wear resistance of Mo coatings is better by a factor of 2-18 compared with uncoated hardened steel (Ref 1). Molybdenum coatings are known to provide low friction and excellent resistance to scuffing under sliding contact conditions. Because of their excellent tribological characteristics, molybdenum and molybdenum alloy powders have been studied as coating materials for automotive parts such as synchronizer rings, cylinder bores, and piston rings (Ref 2, 3).

In early times, sprayed Mo coatings were prepared by flame spraying of Mo wire. However, Mo coatings prepared by flame spraying have short service life due to severe oxidation during spraying and low cohesive strength (Ref 4). Flame spraying has now been replaced as a preparation method for Mo coatings by plasma spraying. However, plasma-sprayed Mo coatings are relatively soft (<300 HV) and do not possess adequate wear resistance (Ref 5). To improve their wear resistance, the effects of blending elements on the wear resistance of plasma-sprayed coatings have been evaluated. Plasma-sprayed Mo coatings obtained by blending or alloying the feedstock powder with materials such as brass, bronze, Mo$_2$C, NiCrBSi, and TiN have been developed as the focus of recent studies (Ref 2, 6, 7). Although such Mo blend coatings exhibit better tribological performance compared with pure Mo coatings, few exceptional results on Mo coatings have been reported. Therefore, it is imperative to develop new molybdenum blend coatings for use on automotive parts.

MoSi$_2$ has dual characteristics, behaving as both a metal and ceramic. It is well known that MoSi$_2$ is an attractive wear-resistant material for application in room- and high-temperature corrosive and oxidative environments because of its high hardness and elastic modulus (Ref 8, 9). Due to their superior properties, MoSi$_2$ coatings are widely deposited on the surface of various substrates to increase the wear resistance (Ref 10, 11). Therefore, improvement of the tribological properties of sprayed Mo coatings is expected through addition of MoSi$_2$ particles.

However, basic research data on the effects of MoSi$_2$ on the microstructure and tribological properties of thermally sprayed Mo coatings are sparse. In the present study, pure Mo coatings and Mo blend coatings, where the Mo powder was blended with MoSi$_2$ powder, were fabricated by atmospheric plasma spraying (APS). Their microstructure, hardness, bond strength, wear properties, and friction coefficient were evaluated.

Jianhui Yan, Zheyu He, Yi Wang, Jingwen Qiu, and **Yueming Wang**, Hunan Provincial Key Defense Laboratory of High Temperature Wear Resisting Materials and Preparation Technology, Hunan University of Science and Technology, Xiangtan, People's Republic of China. Contact e-mail: yanjianhui88@163.com.

2. Experimental Procedures

2.1 Feedstock Powder

Commercial Mo powder (SY-211, 38-74 μm; Beijing Sunspraying Technology Co. Ltd.) and self-manufactured

MoSi$_2$ powder (38-74 μm) were used in this investigation. The MoSi$_2$ powder was prepared by a spray drying process with subsequent vacuum treatment; the detailed preparation process is available in literature (Ref 12). Both the commercial Mo powder and the self-manufactured MoSi$_2$ powder were spherical and porous, as shown in Fig. 1(a-d). Mo coating was fabricated from pure Mo powder. The mixed powder applied for spraying of MoSi$_2$-Mo composite coatings comprised 30 wt.% MoSi$_2$ and 70 wt.% Mo powder, mechanically mixed for 5 h prior to spraying.

2.2 Coating Preparation

Low-carbon steel was used as substrate, being grit-blasted with alumina abrasive under 0.6 MPa pressure then cleaned with acetone before the plasma spraying process. The surface roughness of the blasted low-carbon steel was $R_a = 2.2$ μm. Coatings were prepared on low-carbon steel substrate using APS equipment (APS-2000, China) with a plasma spray gun (PQ-1S), copper anode (nozzle), and tungsten cathode (provided by Beijing Aeronautical Manufacturing Technology Research Institute Manufacturer of China). Argon combined with hydrogen was used as plasma forming gas. The primary spraying parameters for the MoSi$_2$-Mo and Mo coatings were the same, as listed in Table 1. Air cooling was applied on the back side of the substrate to avoid overheating during the spraying process. The coating thickness was about 260 μm.

2.3 Testing of Mechanical Properties

Microhardness measurements were carried out on polished cross-sections using a digital micro-Vickers hardness tester (HVS-1000, Jinan Liangong Testing Technology Corporation of China) with a load of 0.49 N (50 g) for 15 s. Each sample was tested 20 times at different points, with the average value taken as its hardness value. The bond strength test was carried out according to ASTM C633 using an Instron 3369 electronic universal testing machine. The samples for tensile bond strength testing were glued using epoxy (E-7, provided by Shanghai Research Institute of Synthetic Resins, China); the bond strength of the epoxy in the C633 test configuration is 65 MPa. Tensile load was applied at constant loading rate of 1 mm/min. The bond strength was calculated by dividing the failure load by the cross-sectional area. Five specimens were used for each test, with the average value reported as the bond strength.

2.4 Friction and Wear Testing

Wear tests were carried out using a ball-on-disk tribometer (HSR-2M, China) in air environment at room temperature; a schematic diagram of the wear tester is shown in Fig. 2. The wear test method involved a steel ball (5 mm diameter, 48 HRC, $R_a = 0.8$ μm) that was slid against a flat specimen in linear back-and-forth sliding motion with load of 10, 20, 30, and 40 N. The reciprocating wear tests, which lasted for 60 min, were performed under dry conditions with the following test parameters: stroke
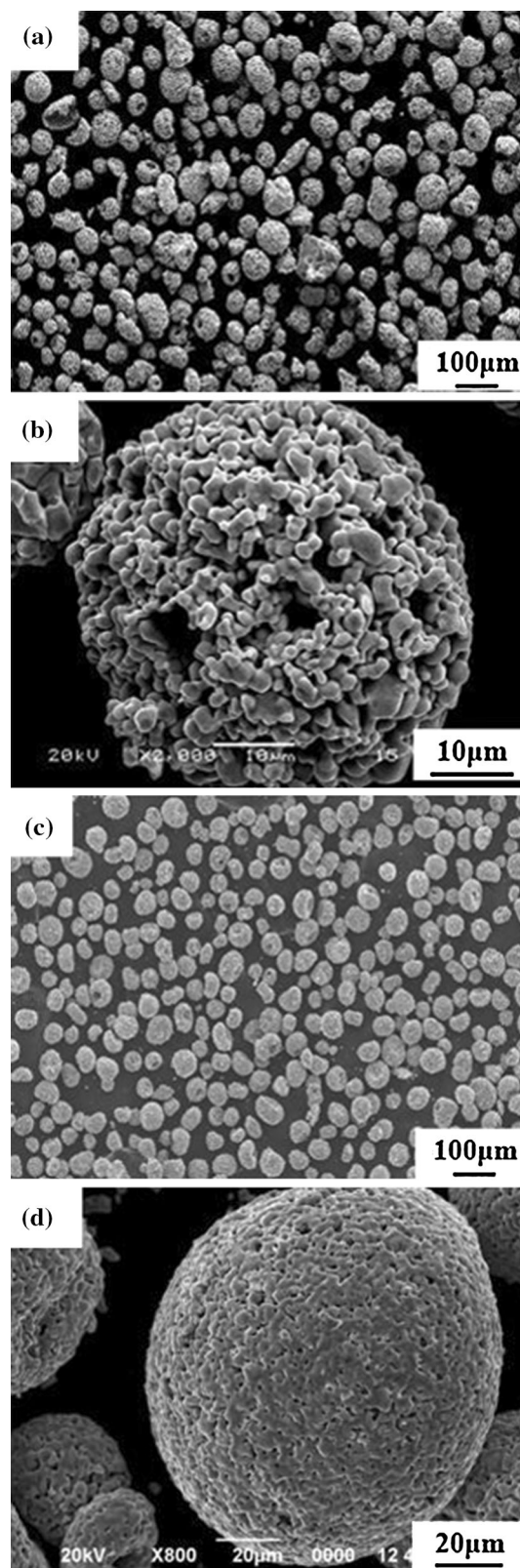

Fig. 1 SEM morphology of sprayed powders: (a) overall morphology of Mo powder, (b) morphology of single Mo particle, (c) overall morphology of MoSi$_2$ powder, and (d) morphology of single MoSi$_2$ particle

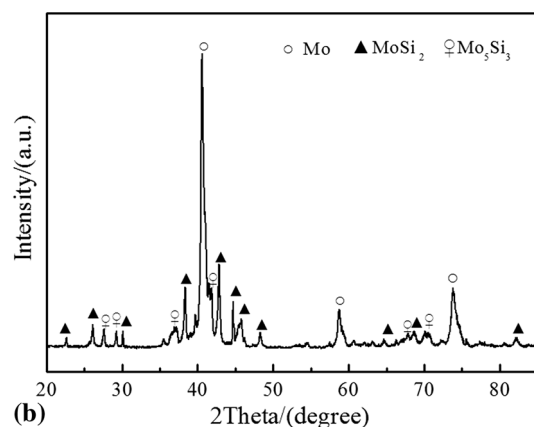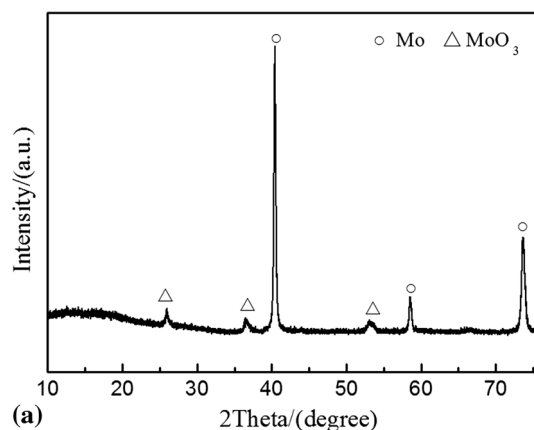**Table 1 Atmospheric plasma spraying parameters for the two coatings**

Spraying parameter	Value
Ar, L/min	45
H_2, L/min	6.5
Current, A	500
Power, kW	32.5
Powder feed rate, g/min	60-65
Powder gas flow rate, L/min	4.0
Spraying distance, mm	110
Torch traverse speed, mm/s	60
Pass spacing, mm	200
Overall number of cycles	16
Cooling air, MPa	0.5
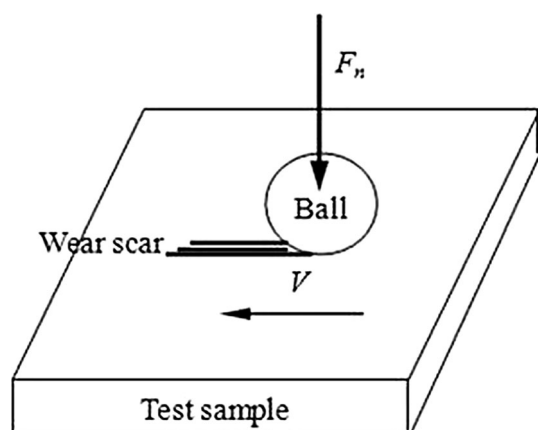
Fig. 2 Schematic diagram of wear test

Fig. 3 XRD patterns of coatings: (a) Mo coating, and (b) $MoSi_2$-Mo coating

length of 5 mm, speed of 50 mm/s, and stroke frequency of 5 Hz. The overall sliding distance was 1.8×10^5 mm. The friction coefficient was dynamically recorded by automatic online measurement. For wear testing, the surface of the coating was ground using different SiC papers to surface roughness R_a of about 0.2-0.4 μm. The wear track morphology and wear volume loss of the coatings were analyzed using a three-dimensional surface profiler (NanoMap-500LS, USA). The wear rate of the coatings was calculated according to the following formula: wear rate = wear volume (mm^3)/load (N) × distance traveled (m).

2.5 Characterization of Coating Microstructure

The phase composition of the coatings was characterized by x-ray diffraction (XRD) analysis using Cu K_α radiation (D8 Discover 2500, Bruker Corporation). The surface and cross-sectional morphologies of the coatings were observed using a scanning electron microscope (SEM, JSM-6380LV, JEOL) equipped with energy-dispersive spectroscopy (EDS). The porosity of the coatings was evaluated by image analysis of SEM images (at magnification of 500×) of the cross-section of polished samples. For each cross-section, 15 images were measured.

3. Results and Discussion

3.1 Phase Composition and Microstructure of Coatings

XRD patterns of the Mo coating and the $MoSi_2$-Mo composite coating are shown in Fig. 3. The Mo coating was composed of Mo with trace MoO_3 phase, whereas the $MoSi_2$-Mo coating consisted of Mo, $MoSi_2$, and Mo_5Si_3 phases. The presence of MoO_3 phase in the Mo coating and Mo_5Si_3 phase in the $MoSi_2$-Mo composite coating is supposed to be caused by oxidation of Mo and $MoSi_2$ particles during the plasma spraying process in air (Ref 13, 14).

Figure 4 shows SEM micrographs of the surface and cross-section of the two as-sprayed coatings. As displayed in Fig. 4(a, b), it is clearly visible that the top surface of both the Mo and $MoSi_2$-Mo coatings was constituted of well-flattened splats, insufficiently flattened protuberances with some degree of surface roughness, spherical features, and many pores, being typical characteristics of plasma-sprayed coatings. The spherical particles observed at the surface of the coatings are believed to be redeposited droplets formed by "splashing" of spray particles upon surface impact.
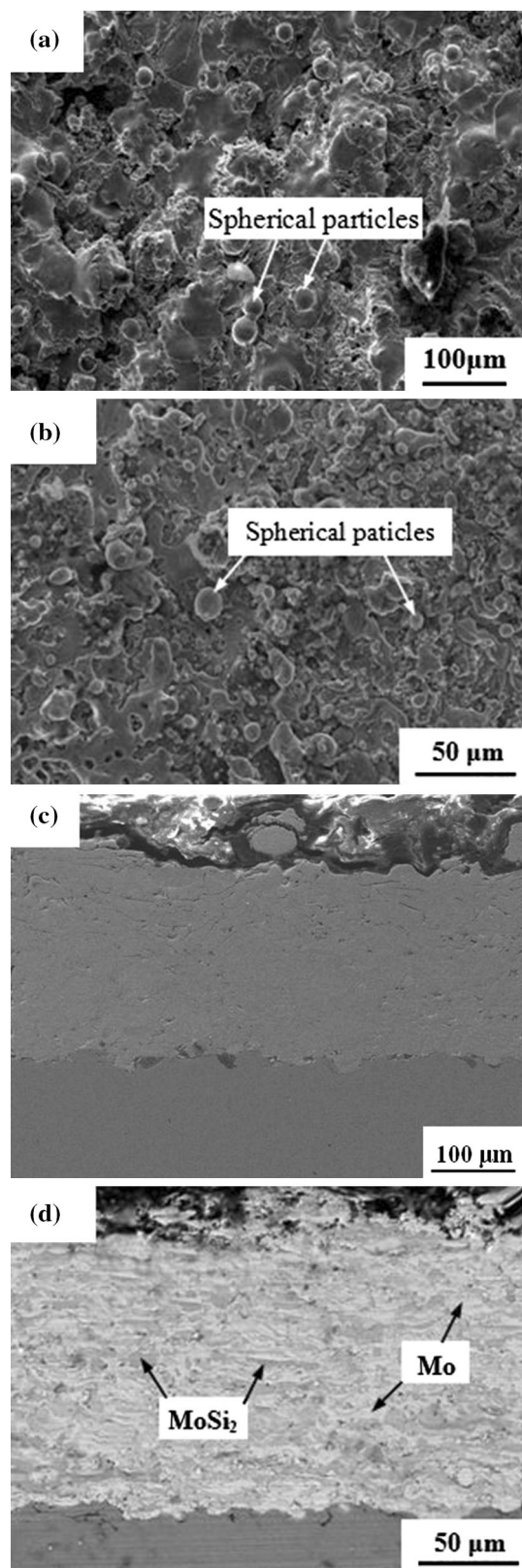
Fig. 4 SEM microstructure of as-sprayed coatings: (a) surface morphology of Mo coating, (b) surface morphology of MoSi$_2$-Mo coating, (c) cross-sectional morphology of Mo coating, and (d) cross-sectional morphology (BSE) of MoSi$_2$-Mo coating

Figure 4(c) shows a cross-sectional image of the as-sprayed Mo coating. The Mo coating was composed of a lamellar structure. During the plasma spraying process, molten particles impact on the surface of the substrate, then deform, solidify, and transform into lamellae, which then pile up one by one to build the lamellar structure of the coating. Some pores and microcracks were also observed in the Mo coating. The overall porosity of the as-sprayed Mo coating was about 7.6 ± 0.4%. Generally, the pores in the sprayed coating included large pores between lamellae and small pores within flattened particles. During the plasma spraying process, expanding gases entrapped in closed pores between lamellae may evacuate to leave large pores in the coating (Ref 15), while the small pores within flattened particles result from shrinkage of solidified particles (Ref 16). As the spray gun was moved over the substrate, the surfaces of the lamellae were subjected to the action of the environment, i.e., cooling and oxidation. The Mo coating contained some microcracks, which are supposed to be caused by residual internal stresses during the cooling process.

A cross-sectional backscattered electron (BSE) image of the MoSi$_2$-Mo coating is shown in Fig. 4(d), showing MoSi$_2$ particles distributed relatively homogeneously in the Mo matrix of the coating. Some insufficiently flattened MoSi$_2$ particles as well as pores and microcracks were also observed in the MoSi$_2$-Mo coating. The mismatch in coefficient of thermal expansion (CTE) between Mo $(6.7 \times 10^{-6}/K)$ and MoSi$_2$ $(9.4 \times 10^{-6}/K)$ usually produces stresses during the cooling process, leading to microcracks (Ref 17). The MoSi$_2$-Mo coating had a relatively dense structure with porosity of 8.8 ± 0.6%, and the MoSi$_2$ particles showed good interfacial bonding with the Mo matrix.

3.2 Bond Strength and Microhardness of Coatings

The bond strength of the two kinds of coating on low-carbon steel substrate is presented in Table 2. The bond strength of the as-sprayed Mo coating was about 42.2 ± 3.2 MPa, whereas that of the MoSi$_2$-Mo coating was about 34.6 ± 2.8 MPa. With addition of 30 wt.% MoSi$_2$ particles into the Mo coating, the bond strength of the as-sprayed Mo coating was remarkably decreased. After the bond strength test, the separated surfaces from all adhesion test samples revealed that the two types of coating did not separate cohesively at splat boundaries but rather exhibited adhesive failure at the coating-substrate boundary, revealing that the bond strength between splats was greater than that between the coating and substrate. The metal Mo has good bonding performance with other materials (Ref 18). When Mo powder is used for spraying, the particles may be sufficiently melted and strongly ad-

Table 2 Bond strength and microhardness of as-sprayed coatings

Coating	Bond strength (MPa)	Microhardness (HV$_{50}$)
Mo	42.2 ± 3.2	308 ± 8
MoSi$_2$-Mo	34.6 ± 2.8	489 ± 10

here to the rough substrate surface. For the MoSi$_2$-Mo coating, insufficiently flattened MoSi$_2$ particles appeared, adversely affecting the mechanical interlocking between splats or between the coating and substrate. The adhesive strength of pure MoSi$_2$ coatings prepared by APS is no more than 20 MPa (Ref 14). Thus, with addition of MoSi$_2$ particles to the Mo coating, the bond strength was slightly decreased.

The measured microhardness values for the two coatings are presented in Table 2. The microhardness of the Mo coating was about 308 ± 8, whereas that for the MoSi$_2$-Mo coating was about 489 ± 10. The MoSi$_2$ intermetallic has dual characteristics, behaving as both a metal and ceramic. It is well known that MoSi$_2$ is an attractive wear-resistant material for application in room- and high-temperature corrosive and oxidative environments because of its high hardness and elastic modulus (Ref 8-11). In general, cracks, porosity, and adhesion between splats decrease the microhardness of sprayed coatings (Ref 19). However, pure MoSi$_2$ has hardness of about 8.9 GPa (HV). The intermetallic compound MoSi$_2$ plays a role in increasing the microhardness of the Mo coating. With addition of 30 wt.% MoSi$_2$ particles into the Mo coating, the microhardness of the as-sprayed MoSi$_2$-Mo coating was increased by 58.8% compared with the as-sprayed Mo coating.

3.3 Friction Coefficient and Wear Rate

Figure 5 shows the evolution of the friction coefficient for the two kinds of coating as a function of sliding time under different applied loads. As shown in Fig. 5(a), the friction coefficient of the Mo coating against steel ball initially increased and then reached a steady state. The friction coefficient for the MoSi$_2$-Mo coating followed a similar general trend with respect to sliding time. The steady-state friction coefficient value for the Mo coating ranged from 0.75 to 1.08, whereas that for the MoSi$_2$-Mo coating increased from 0.52 to 0.74 as the applied load was increased from 10 to 40 N. Under the same test condition, the friction coefficient of the MoSi$_2$-Mo coating was lower than that of the Mo coating, indicating that addition of MoSi$_2$ can reduce the friction coefficient of the Mo coating at room temperature under dry conditions.

Figure 6 shows the profile curves of wear scratches for the Mo and MoSi$_2$-Mo coatings under applied load of 40 N. The wear profiles of the two coatings for the other applied loads are not shown here for the sake of brevity. It can be seen that the width and depth of the scratches on the Mo coating were approximately 1080 and 20 μm, respectively. For the MoSi$_2$-Mo coating, they were about 950 μm and 15 μm, respectively. Figure 7 shows the wear rate of the two coatings as a function of applied load. It can be seen that the wear rate of the two coatings gradually increased with increasing applied load. At load of 40 N, the wear rate of the Mo coating with and without MoSi$_2$ was 1.82×10^{-5} and 2.90×10^{-5} mm^3 (N m)$^{-1}$, respectively. It can be concluded that the wear resistance of the MoSi$_2$-Mo coating is superior to that of the Mo coating.
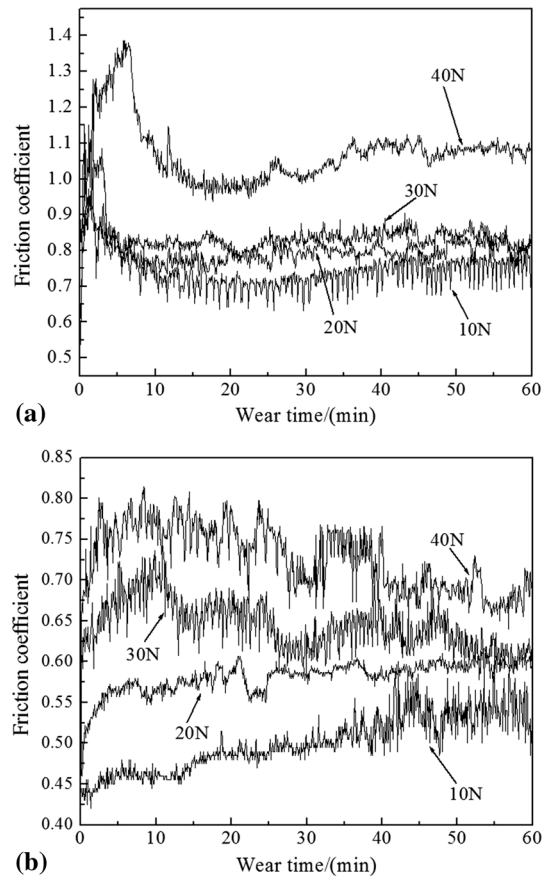

Fig. 5 Friction coefficient of as-sprayed coatings under different applied loads: (a) Mo coating, and (b) MoSi$_2$-Mo coating

3.4 Micrographs of Worn Surface

These micrographs represent the steady-state wear conditions, since they were taken at the end of testing. Figure 8 shows SEM images of the Mo coating treated at loads of 10 and 40 N under dry conditions. An obvious wear scar can be observed on the worn surface of the Mo coating in Fig. 8(a, c), and splat delamination, pits, local plastic deformation, and cracks are also seen in Fig. 8(b, d). The load applied to the steel counterpart causes an abrasive effect on the surface of the Mo coating, thus plastic deformation zones are formed. Wear debris in the form of flakes is generated during sliding of the coated samples against the steel counterpart. The pits are easily filled with wear debris during the test. As displayed in Fig. 9(a-d), the extent of plastic deformation and the number of cracks, splat fractures, delaminations, and pits were found to increase with increasing applied load.

SEM micrographs of the worn surface of the MoSi$_2$-Mo coating under loads of 10 and 40 N are shown in Fig. 9. As seen in Fig. 9(a, c), the wear scar width increases with increase of the applied load. Comparing with the Mo coating, the worn surface of the MoSi$_2$-Mo coating showed similar characteristics such as local plastic deformation, cracks, delamination, and pits (Fig. 9a-d). Under the same
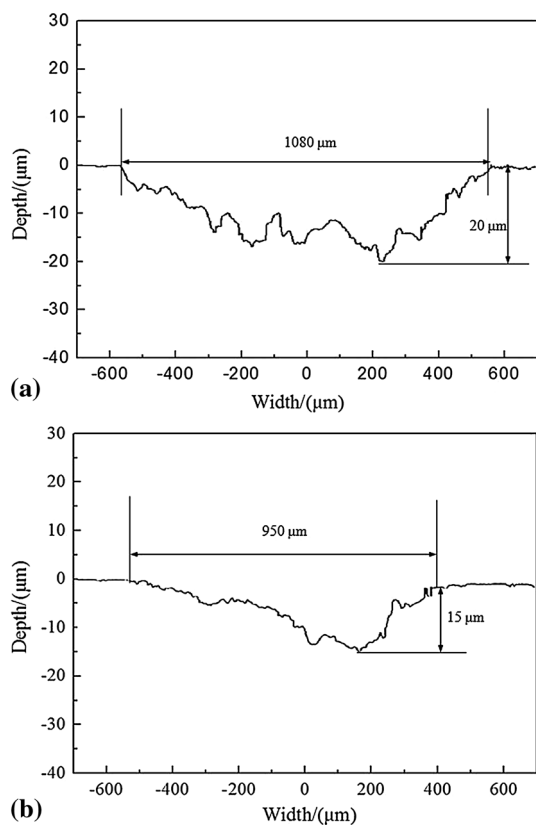
Fig. 6 Profile curves of wear scratches under applied load of 40 N: (a) Mo coating, and (b) MoSi$_2$-Mo coating
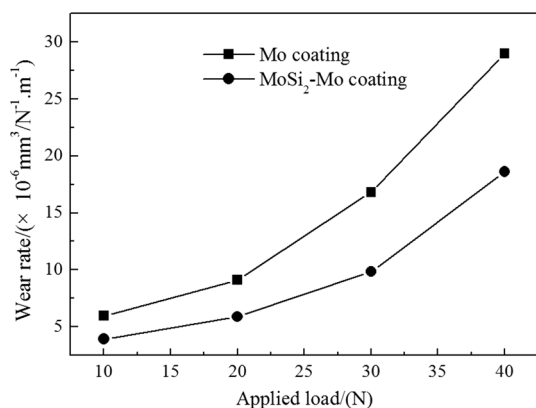

Fig. 7 Wear rate of two coatings under different applied loads

wear test conditions, the width and depth of the wear scar for the MoSi$_2$-Mo coating were smaller than observed on the worn surface of the unreinforced Mo coating, indicating that the MoSi$_2$-Mo coating had better wear resistance.

To further illustrate the wear mechanisms of the coatings, wear tracks were analyzed by EDS. The results of EDS analysis at zones A and B in Fig. 8(d) and zones C and D in Fig. 9(d) are listed in Table 3. These results show that the worn surface of the Mo and MoSi$_2$-Mo coatings
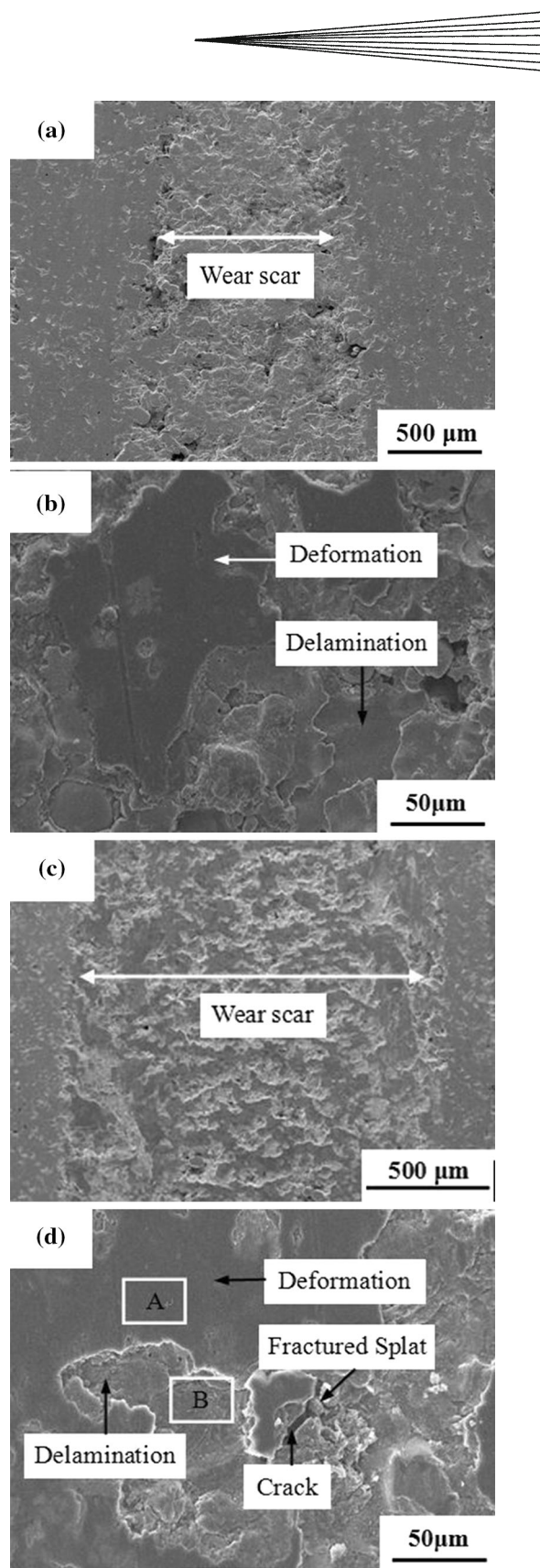

Fig. 8 SEM micrographs of worn surface of Mo coating tested at different loads: (a) 10 N and (b) high-magnification morphology of (a), (c) 40 N, and (d) high-magnification morphology of (c)

Fig. 9 SEM micrographs of worn surface of MoSi$_2$-Mo coating tested at different loads: (a) 10 N and (b) high-magnification morphology of (a), (c) 40 N and (d) high-magnification morphology of (c)
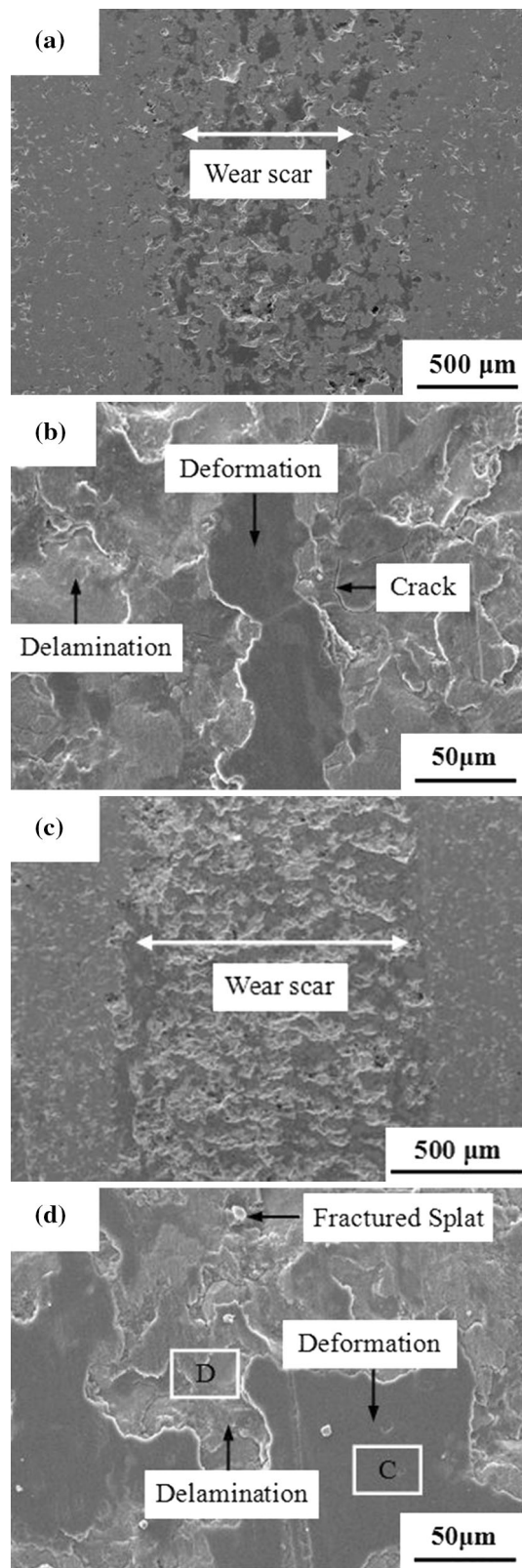
Table 3 Elemental composition of different zones in Fig. 8(d) and 9(d)

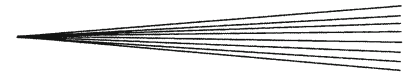| Zone	Element (at.%)		
	Fe	Mo	O
A	5.6	86.2	8.2
B	0	100	0
C	4.8	87.9	7.3
D	0	100	0

contained Fe, Mo, and O elements, indicating that oxidation occurred during the wear process. The temperature on the contact surface increased with the reciprocating motion, leading to oxidation reaction between metals and oxygen. The presence of Fe element on the coating surface implies that adhesion wear occurred between the coating and steel ball. The main wear mechanisms of the two coatings are therefore associated with plastic deformation, oxidation, and adhesion wear.

In general, the friction and wear behavior of a material depends on its microstructure, microhardness, and friction characteristics as well as environmental conditions (Ref 20). The microstructure of the Mo and MoSi$_2$-Mo coatings (Fig. 4) indicates that some pores and intersplat cracks were present. When the surface of a plasma-sprayed coated sample is in contact with the surface of the counter face, the coating experiences severe stress. This stress drives propagation of intersplat cracks until the splats are no longer attached and easily removed. Thus, splat fracture and particle pullout take place at such sites, finally leading to material loss from the coating surface in the form of delamination.

The fracture and delamination of splats varied with the wear load, considerably affecting the wear rate of the coating. As the load was increased from 10 to 40 N, the fracture and delamination of splats became more severe (Fig. 8, 9), therefore the wear rates of the two coatings increased. The wear properties of a material are often related to its hardness. As mentioned above, strengthening with MoSi$_2$ can provide the Mo coating with high hardness (Table 2). During dry sliding of the unreinforced Mo coating, the steel counterpart can penetrate into the Mo coating, resulting in large removal of material from the surface by plowing action. In the case of the composite coating, the contact interaction between the coating surface and counterpart is controlled by the reinforcing particles (Ref 21). During the test, load-bearing MoSi$_2$ particles protruding from the coating surface reduce direct contact between the molybdenum part and steel ball, thereby preventing a greater extent of wear.

4. Conclusions

Mo coatings with or without incorporated MoSi$_2$ particles were fabricated on low-carbon steel substrate by APS, and their microstructure, mechanical properties, and tribological properties were investigated under dry con-

ditions. Lamellar structure, small pores, and microcracks were observed in the Mo and MoSi$_2$-Mo coatings. The MoSi$_2$ phase was homogeneously distributed in the Mo matrix for the MoSi$_2$-Mo coating. Addition of MoSi$_2$ particles increased the porosity of the as-sprayed Mo coating, thus decreasing the coating-substrate adhesion strength. However, the MoSi$_2$ particles could also increase the hardness of the Mo coating. Addition of MoSi$_2$ particles could effectively reduce the friction coefficient and wear rate of the Mo coating. This increase in the wear resistance is believed to be related to the enhanced hardness. The main wear mechanisms of the two coatings were local plastic deformation, delamination, oxidation, and adhesion wear.

Acknowledgments

References

1. Z. Liu and M. Hua, Wear Transition and Mechanism in Lubricated Sliding of a Molybdenum Coating, *Tribol. Int.*, 1999, **32**(9), p 499-506

2. B. Hwang, J. Ahn, and S. Lee, Effects of Blending Elements on Wear Resistance of Plasma-Sprayed Molybdenum Blend Coatings Used for Automotive Synchronizer Rings, *Surf. Coat. Technol.*, 2005, **194**(2-3), p 256-264

3. S. Usmani and S. Sampath, Time-Dependent Friction Response of Plasma-Sprayed Molybdenum, *Wear*, 1999, **225-229**, p 1131-1140

4. S.C. Modi and Eklavya Calla, A Study of High-Velocity Combustion Wire Molybdenum Coatings, *J. Therm. Spray Technol.*, 2001, **10**(3), p 480-486

5. S. Sampath and S.F. Wayne, Microstructure and Properties of Plasma-Sprayed Mo-Mo$_2$C Composites, *J. Therm. Spray Technol.*, 1994, **3**(3), p 282-288

6. L. Prchlik, J. Gutleber, and S. Sampath, Deposition and Properties of High-Velocity-Oxygen-Fuel and Plasma-Sprayed Mo-Mo$_2$C Composite Coatings, *J. Therm. Spray Technol.*, 2001, **10**(4), p 643-655

7. D. Debasish, S. Mantry, D. Behera, and B.B. Jha, Improvement of Microstructural and Mechanical Properties of Plasma Sprayed Mo Coatings Deposited on Al-Si Substrates by Pre-mixing of Mo with TiN Powder, *High Temp.*, 2014, **52**(1), p 19-25

8. J.A. Hawk and D.E. Alman, A Comparative Study of the Abrasive Wear Behavior of MoSi$_2$, *Scr. Metall. Mater.*, 1995, **32**, p 725-730

9. J.A. Hawk and D.E. Alman, Abrasive Wear Behavior of a Brittle Matrix (MoSi$_2$) Composite Reinforced with a Ductile Phase (Nb), *Wear*, 2001, **251**(1-12), p 890-900

10. J.H. Yan, Z. Zhang, L.F. Liu, H.M. Xu, and Z.Y. Mao, Effect of Nano-ZrO$_2$ on the Microstructure, and High Temperature Tribological Properties of MoSi$_2$ Coating, *J. Therm. Spray Technol.*, 2013, **22**(6), p 873-881

11. P.Q. La, Q.J. Xue, and W.M. Liu, Tribological Properties of MoSi$_2$-MoS$_2$ Coatings Coupling with SAE 52100 Steel Under Reciprocating Sliding, *Surf. Coat. Technol.*, 2001, **135**(2-3), p 118-125

12. J.H. Yan, J.J. Xu, R.U. Din, Y. Wang, and L.F. Liu, Preparation of Agglomerated Powders for Air Plasma Spraying MoSi$_2$ Coating, *Ceram. Int.*, 2015, **41**, p 10547-10556

13. J.H. Yan, Y. Wang, L.F. Liu, Y.M. Wang, and F. Chen, Preparation of Protective MoSi$_2$ Coating on Niobium Substrate, *J. Therm. Spray Technol.*, 2015, **24**(6), p 1093-1099

14. J.H. Yan, L.F. Liu, Z.Y. Mao, H.M. Xu, and Y.M. Wang, Effect of Spraying Powders Size on the Microstructure, Bond Strength, and Microhardness of MoSi$_2$ Coating Prepared by Air Plasma Spraying, *J. Therm. Spray Technol.*, 2015, **24**(6), p 934-939

15. X.B. Zhao and Z.H. Ye, Microstructure and Wear Resistance of Molybdenum Based Amorphous Nanocrystalline Alloy Coating Fabricated by Atmospheric Plasma Spraying, *Surf. Coat. Technol.*, 2013, **228**(S1), p 266-270

16. V.V. Sobolev and J.M. Guilemany, Investigation of Coating Porosity Formation During High Velocity Oxy-Fuel (HVOF) Spraying, *Mater. Lett.*, 1994, **18**(5-6), p 304-308

17. J.K. Yoon, G.H. Kim, J.Y. Byun, J.K. Lee, and J.S. Kim, Formation of Crack-Free MoSi$_2$/α-Si$_3$N$_4$ Composite Coating on Mo Substrate by Ammonia Nitridation of Mo$_5$Si$_3$ Layer Followed by Chemical Vapor Deposition of Si, *Surf. Coat. Technol.*, 2003, **165**(1), p 81-89

18. X.H. Wang, F. Han, X.M. Liu, S.Y. Qu, and Z.D. Zou, Effect of Molybdenum on the Microstructure and Wear Resistance of Fe-Based Hard Facing Coatings, *Mater. Sci. Eng. A*, 2008, **489**(1-2), p 193-200

19. X. Fei, Y. Niu, H. Ji, L. Huang, and X. Zheng, A Comparative Study of MoSi$_2$ Coatings Manufactured by Atmospheric and Vacuum Plasma Spray Processes, *Ceram. Int.*, 2011, **37**(3), p 813-817

20. Z.J. Yin, S.Y. Tao, X.M. Zhou, and C.X. Ding, Microstructure and Mechanical Properties of Al$_2$O$_3$-Al Composite Coatings Deposited by Plasma Spraying, *Appl. Surf. Sci.*, 2008, **254**(6), p 1636-1643

21. M. Amiriyan, H.D. Alamdari, C. Blais, S. Savoie, R. Schulz, and M. Gariépy, Dry Sliding Wear Behavior of Fe$_3$Al and Fe$_3$Al/TiC Coatings Prepared by HVOF, *Wear*, 2015, **342-343**, p 154-162